Available online at www.sciencedirect.com

SciVerse ScienceDirect

Proceedings of the Combustion Institute 34 (2013) 1869–1876

Proceedings of the Combustion Institute

www.elsevier.com/locate/proci

Nanostructure and oxidative properties of soot from a compression ignition engine: The effect of a homogeneous combustion catalyst

Dongke Zhang *, Yu Ma, Mingming Zhu

Centre for Energy (M473), The University of Western Australia, 35 Stirling Highway, Crawley, WA 6009, Australia

Available online 18 June 2012

Abstract

This study examined the influence of an iron-based homogeneous combustion catalyst on the oxidative behaviour and nanostructural characteristics of soot emitted from a single-cylinder compression ignition engine. The catalyst was homogeneously added into a commercial diesel as the reference at ultra low dosage ratios. Smoke opacity was measured using a smoke opacimeter in the engine exhaust stream to indicate the overall soot emission intensity. Soot particles were also sampled while the engine was maintained in steady-state operations and fuelled with the reference diesel and the catalyst treated fuels, respectively. The soot samples were subjected to thermogravimetric analysis (TGA) to study their oxidation reactivities in air, and transmission electron microscopy (TEM) for morphological characterisations. The smoke opacity results showed 7.3–39.5% less soot emissions when the catalyst was applied, depending on the catalyst dosage ratio. The TGA results revealed that soot from the catalyst treated fuels possessed higher oxidative reactivity as indicated by ignition at lower temperatures and faster oxidation rates than those of soot from the reference diesel. This tendency was more remarked as the catalyst dosage ratio increased. Subsequent TEM imaging analyses observed that the irregularly shaped, aggregated soot particles were made of a number of spherical primary particles. Smaller and more narrowly-distributed primary soot particles with the catalyst treated fuels than those of the reference diesel were evident. High-resolution TEM imaging revealed graphitic crystallite structures of the soot samples from both catalyst-treated and -untreated fuels with no obvious variations in the nuclei core areas, suggesting that the internal structure of the soot was not affected by the catalyst. It was evident that iron ions from the catalyst were more involved in the soot oxidation process, rather than in the early soot formation stage, and eventually resulted in smaller and narrowly-distributed primary soot particles.

Keywords: Compression ignition engine; Homogeneous combustion catalyst; Nanostructure; Soot; Oxidation

1. Introduction

Compression ignition (CI) diesel engines are increasingly favoured for surface transportation, heavy machinery and remote power generation compared to spark-ignition gasoline engines, due to their inherently higher fuel efficiency and durability. However, diesel engines generate significant amounts of particulate matter (PM) emissions, commonly known as soot, which threaten the air quality and human health, particularly in urban environments [1–3]. Typically, the diesel soot

* Corresponding author. Fax: +61 8 6488 7235.
E-mail address: dongke.zhang@uwa.edu.au (D. Zhang).

1540-7489/$ - see front matter © 2012 The Combustion Institute. Published by Elsevier Inc. All rights reserved.
http://dx.doi.org/10.1016/j.proci.2012.05.096

particles are composed of agglomerated primary particles with absorbed unburnt hydrocarbons and inorganic species on their surfaces [1,4]. Many toxicological and epidemiological investigations have been reported that PM can accumulate in the respiratory system and even penetrate the cell membranes to induce inheritable mutations [4,5]. Therefore, strict diesel PM emission regulations have been imposed by many governments and will become far more stringent in the future [6].

Numerous efforts have been devoted to controlling diesel PM emissions by modifying engine design and fuel injection and by reforming fuel properties to improve the combustion process [3,6,7]. Among these, the use of metallic-based combustion catalyst is an attractive approach and has shown significant benefits in reduced fuel consumption and lowered diesel exhaust emissions with no need for engine modifications [8–12]. On the molecular level, the catalysts consist of a metallic part as the active material that promotes fuel combustion and an organic part to make the catalysts soluble in diesel fuels, thus the term homogeneous combustion catalysts (HCC).

Various laboratory and modelling studies have been reported in the literature exploring the effects of iron-based compounds on PM reductions in premixed [13] or diffusion flames [14], drop tube furnaces [15], boilers [16] and diesel engines [17,18], in the forms of iron pentacarbonyl ($Fe(CO)_5$), ferrocene ($Fe(C_5H_5)_2$), iron naphthenate, iron chloride ($FeCl_3$). Shayeson [19] detected the smoke reduction in a jet engine using an iron-based catalyst. Braun et al. [20] investigated the microstructure and molecular structure of soot samples from ferrocene doped diesel using near edge X-ray absorption fine structure (NEXAFS) spectroscopy and X-ray scattering and found that the addition of ferrocene dramatically affected soot formation and its graphitic structure. Marsh et al. [15] proposed four possible ways in which an iron catalyst may suppress PM emissions: (1) by inhibiting particle formation; (2) by enhancing fuel vaporisation and premixing; (3) by increasing ignition delay which allowed more time for fuel mixing before the flame is established; and (4) by catalytically promoting the oxidation of soot particles. Hahn et al. [14] studied isooctane diffusion flames with iron pentacarbonyl addition and found that rather than affecting soot particle inception and growth, iron was more effective in enhancing the rate of soot oxidation during burnout resulting in a two-thirds reduction in the overall soot emissions.

The present work involved a novel Fe-based HCC, which consisted of ferrous picrate as the active ingredient in a complex solution of short-chain alkyl benzenes to form a continuous phase with diesel. Previous field trials and our laboratory studies [21–23] have confirmed the significant effects of the ferrous picrate catalyst (FPC) in improving fuel economy and reducing smoke emissions. However, its impacts in the characteristics of soot particles from diesel engines remain unknown.

This contribution reports an experimental study, as a part of our continuing efforts, to examine the differences in the oxidation reactivities and morphological properties of the soot emitted from a diesel engine fuelled with diesel with and without FPC additions and to understand the mechanisms of FPC catalysts in diesel combustion in compression ignition engines.

2. Experimental

2.1. Laboratory engine system

Experiments were carried out using a four-stroke, single cylinder, direct injection diesel engine (AET Ltd.) which was coupled to a Zöllner TypeA-100 electric dynamometer for load control. The engine specifications are listed in Table 1 and the details of the engine system can be found elsewhere [22]. A commercial standard No.2 diesel from a local service station (Caltex Australia Ltd.) was employed as the reference diesel and a ferrous picrate catalyst was obtained from Fuel Technology Pty. Ltd. The catalyst was added in the diesel at dosage ratio of 1:15,000, 1:10,000, 1:5000 and 1:1000 (catalyst to fuel, vol./vol.), respectively. Smoke opacity was measured with a Bosch RTM 430 infrared opacimeter to indicate the overall PM emissions while the engine operated under full load and various speeds ranging from 2800 rpm to 3600 rpm with a 200 rpm interval. Prior to each test, the engine was allowed to operate under a set of specified conditions for 1 h in order to ensure steady state was reached. When a different fuel was tested, the engine was run with the new fuel for at

Table 1
Specifications of the laboratory diesel engine and instrumentation.

Engine model	Yanmar L48AE-DG
Engine type	Four stoke, direct injection, single cylinder
Cylinder number	1
Bore (mm) × stroke (mm)	70 × 55
Total displacement (L)	0.211
Compression ratio	19.9
Maximum output (kW)	3.5
Rated speed (rpm)	3600
Injection timing	14 ± 1 BTDC (before top dead centre)
Injection pressure	19.6 MPa

least 30 min to eliminate the effect of the fuel in the previous test.

2.2. Thermogravimetric analysis (TGA)

Soot samples were directly collected from the exhaust pipe when the engine reached a steady-state engine condition at the speed of 3200 rpm and 5.5 N m load. A 90 mm diameter glass fibre filter paper (Whatman GF/A, 1.6 μm pore size diameter) was located in the exhaust path for 3 h during each collection. A schematic diagram of the soot collection arrangements is illustrated in Fig. 1. The soot sample was scratched off from the filter paper and stored in a desiccator for further analysis.

Non-isothermal TGA tests were performed using a TGA analyser (SDT-Q600, TA instrument) which allowed simultaneous measurements of weight loss and heat flow as a function of time or temperature. 5.5–6.0 mg of a soot sample was loaded in the alumina crucible and heated in ultra high purity air (flow rate of 15 ml min^{-1}) from 25 to 700 °C at a heating rate of 10 °C min^{-1}. Each analysis was repeated three times to ensure the reproducibility. The TG-DSC (the mass loss and differential scanning calorimetry or heat flow) and TG-DTG (the differential mass loss) curves were obtained to reveal the key thermal behaviour, and the oxidation kinetic parameters were calculated from TGA data following the method described in Ref. [24], as also detailed in Section 3.2.2.

2.3. Thermophoretic sampling technique and TEM analysis

A thermophoretic sampling technique, following Dobbins and Megaridis [25], was employed to collect soot particles from the hot exhaust stream, as also shown in Fig. 1. A sampling probe with a stainless steel stop-valve was installed along the exhaust pipe. A 3 mm TEM copper grid (200 mesh, holey carbon film) was attached to a grid holder which was inserted parallel to the exhaust flow for direct collection of soot particles. The grid holder was connected to a step motor which moved the grid holder in and out of the exhaust pipe through the stop-valve to allow the hot soot particles to be deposited on the copper grid. The overall exposure time of the grid for each soot collection was controlled and set to 1 s by the step motor.

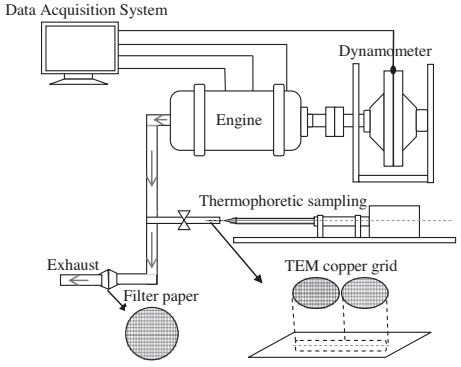

Fig. 1. A schematic of the arrangements for soot sampling and collection.

Soot samples were collected when the engine operated under a fixed condition (3200 rpm and 5.5 N m load) and fuelled with the reference diesel and diesel dosed with FPC at 1:10,000 and 1:1000 ratios, respectively. Three parallel sample grids were taken for each fuel to ensure repeatability. After sample collection, the grids were detached from the grid holder and examined using a high-resolution JEOL 2100 transmission electron microscopy (TEM) at the accelerating voltage of 120 kV to obtain TEM images for further analysis and interpretation. To reveal the soot morphological features such as primary particle diameters and distributions, magnifications in the range of 5000×–50,000× were used and the TEM images were analysed using the DigitalMicrograph software [26,27]. High-resolution TEM images with a 250,000× magnification were obtained to identify the interfacial structure and lattice spacing within the soot particles.

3. Results and discussion

3.1. Particulate emissions

Diesel PM is generated primarily due to incomplete combustion of fuel inside the diesel engines, following very complex mechanisms [1,28,29] and is responsible for the smoke opacity [1]. Smoke opacimeter measures the relative intensity of light that passes through the exhaust stream as an approximate indication of the PM emission levels. Figure 2 illustrates the smoke levels under various engine speed conditions from the reference diesel and the FPC catalyst treated fuels with different dosing ratios, respectively. It is noticed that the smoke emissions were drastically suppressed by the addition of the FPC catalyst and the reduction increased with increasing catalyst dosage ratio, however, levelled off when the catalyst dosage ratio was greater than 1:5000. The reductions in the smoke emissions ranged from 7.3% to 39.5% for the four catalyst treated fuels as compared against the reference diesel.

It is interesting to note that the catalyst was more effective when the engine operated at relatively lower (e.g. 2800 rpm) or higher speeds (e.g. 3400–3600 rpm). At the low engine speed, the in-cylinder temperature was relatively lower, leading

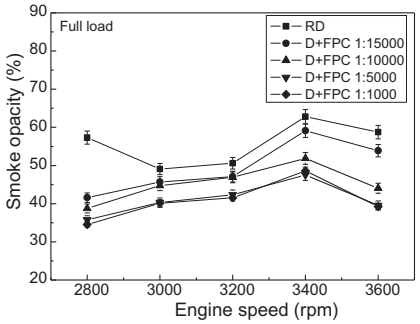

Fig. 2. Variation of the smoke emissions as a function of engine speed for the five fuels tested under the full load conditions.

to incomplete combustion of the fuel and thus the smoke emission increased. At the high speeds, more fuel was injected and expected to burn with short residence times in the engine with a fixed volume (displacement), which also resulted in incomplete combustion and high smoke intensities. However, comparing the smoke opacities of the exhausts of the engine operating with the FPC catalyst treated fuels against that with the reference diesel, it was more obvious when the engine was running under the more inefficient conditions, the FPC catalyst was more effective in reducing the engine smoke emissions.

3.2. TGA analysis and kinetic study of soot oxidation

3.2.1. TGA analysis

Figure 3 presents the TGA data showing the thermal behaviour of the three soot samples collected from the engine operating with the reference diesel and diesel dosed with FPC at ratios of 1:10000 (abbreviated as D + FPC 1:10^4) and 1:1000 (abbreviated as D + FPC 1:10^3), respectively.

The TG-DSC curves in Fig. 3(a) demonstrate that the three soot samples generally exhibited three characteristic mass loss events within the experimental temperature range. The first significant mass loss event occurred at around 150–290 °C with about 50% mass loss, which was related to the evaporation of volatile organic compounds (VOC) adsorbed on the soot particles [24]. The second major mass loss event was observed at approximately 300–500 °C, accompanied by an exothermic heat effect, which accounted for about 30% mass loss and may be attributed to the oxidation of heavy hydrocarbon compounds attached to the surface of the soot particles such as VOC, unburned hydrocarbon and PAH [30]. During this period, the mass loss was similar between the soot samples from the reference diesel and the FPC treated fuels until 500 °C when the major heat release was identified from the oxidation of

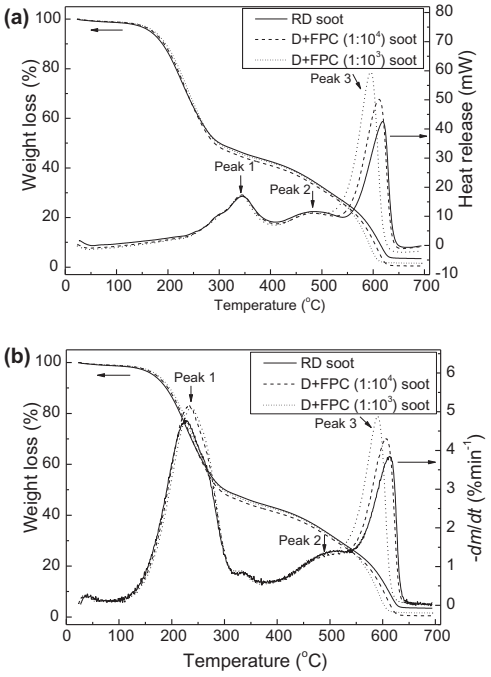

Fig. 3. Comparison of the (a) TG-DSC and (b) TG-DTG curves of the soot samples from the engine operating at 3200 rpm and 5.5 Nm load, and fuelled with diesel with or without FPC catalyst in air.

remaining dry soot particles (primarily graphitic carbon). It was noticed that the heat release peak was shifted towards a lower temperature with increasing the catalyst dosage ratio. The third mass loss event accounting for ca. 15% mass loss occurred at 550–620 °C was caused by the oxidation of the residual carbon. Finally, there were small quantities of ash residues remaining at the conclusion of the TGA tests, accounting for less than 3% of the original sample masses [2].

The respective TG-DTG curves are shown in Fig. 3(b). The three peaks are clearly observable, corresponding to the three mass loss events, respectively, as discussed above. The first sharp peaks related to the light hydrocarbon evaporation and desorption and are similar in shape and peak temperatures at 200–220 °C, except the peaks for the (D + FPC 1:10^4) and (D + FPC 1:10^3) soot samples were higher than that for the reference diesel soot. This suggests that rate of the light hydrocarbon evaporation and desorption from the soot from the FPC treated fuels was faster. The second broad, although less obvious, peaks spread over 450–520 °C are thought to be associated with oxidation of heavier hydrocarbon compounds attached to the soot particles, and thus slower rates and broader peaks. It is interesting to note that the three DTG curves were indistinguishable in the temperature region from 400 to

500 °C until the oxidation of the dry soot began at above 500 °C. This suggests that the iron ions present in the soot had no or little effect in the stage of the oxidation of the adsorbed hydrocarbons. The third sharp peaks at 580–610 °C, however, show two interesting features, that is, the peak increased height and thus the rate of oxidation and shifted towards a lower temperature as the FPC catalyst dosing ratio increased. This suggests once again that the iron ion deposited on the soot from catalyst treated fuel catalysed the soot oxidation causing the soot to react at lower temperatures and at faster rates than the reference diesel soot without iron ions in it.

Further analyses of the DTG curves in the dry soot oxidation region revealed two characteristic temperatures [31], namely, the peak temperature (T_{peak}) and the burnout temperature ($T_{burnout}$). T_{peak} represents the temperature at which the maximum rate of mass loss due to soot oxidation occurs and a lower T_{peak} indicates an easy ignition. $T_{burnout}$ refers to the temperature at which the oxidation is completed. The corresponding T_{peak} and $T_{burnout}$ values of the soot samples from the reference diesel and the two FPC treated fuels are given in Table 2. Note that T_{peak} and $T_{burnout}$ of the soot samples from the two catalyst treated fuels shifted to lower temperatures by ca 10 and 30 °C, respectively, relative to that of the soot from the reference diesel. These results suggest that when the catalyst was added to diesel, the soot became to ignite at a lower temperature and the combustion completed sooner, in other words, the oxidation reactivity of the soot had increased due to the presence of the iron ions. It has been reported that a tiny amount of a transitional metal or metal oxide can drastically increase the oxidation rate of diesel soot [24,32–34]. Miyamoto et al. [34] reported that soot from an iron-doped fuel displayed a rapid mass loss when subjected to combustion in air. Similarly, Bonnefoy et al. [33] attributed an observed increase in the oxidation reactivity of soot from a ferrocene dosed diesel to iron present in the soot. The findings of the present experiments are consistent with these literature reports, albeit, different catalysts were used.

Table 2
Peak and burnout temperatures of the soot samples from diesel with or without the FPC catalyst.

	T_{peak} (°C)	$T_{burnout}$ (°C)
RD soot	615	645
D + FPC (1:10^4) soot	606	635
D + FPC (1:10^3) soot	590	624

T_{peak} – peak temperature from DTG curve of soot oxidation.
$T_{burnout}$ – burnout temperature from DTG curve of soot oxidation.

Table 3
Calculated oxidation kinetic parameters of the soot collected from diesel with or without the FPC catalyst.

Parameters	E_a (kJ mol^{-1})	A (s^{-1})
RD soot	199 ± 3	3.12×10^9
D + FPC (1:10^4) soot	240 ± 2	1.50×10^{12}
D + FPC (1:10^3) soot	242 ± 2	3.37×10^{12}

3.2.2. Estimation of oxidation kinetic parameters

The kinetics of oxidation of the dry soot in the temperature range of 500–600 °C was further studied using the standard kinetic rate equation according to the Arrhenius law:

$$-\frac{dm}{dt} = k \cdot m^n = Ae^{-\frac{Ea}{RT}}m^n \quad (1)$$

where m is the instantaneous mass of a soot sample; t is the reaction time; k is the rate constant of the soot oxidative reaction; A and E_a are the Arrhenius pre-exponential factor and activation energy; T is the absolute temperature of the soot; n is the reaction order and an assumption of $n = 1$ was applied for soot oxidation [35].

A and Ea were calculated from the intercept and the slope of the plot of $ln\left(-\frac{dm}{dt}\frac{1}{m}\right)$ vs. $1/T$, respectively. Knowing A and Ea, the rate constant k at a specific temperature T can be calculated using the Arrhenius equation $\left(k = Ae^{-\frac{Ea}{RT}}\right)$. The calculated kinetic parameters are tabulated in Table 3 and the Arrhenius plots of $\ln k$ vs (1000/T) for the three soot samples are compared in Fig. 4. The activation energy Ea for soot from the FPC treated fuels was 240–242 kJ mol^{-1}, slightly higher than that of the reference diesel soot at 199 kJ mol^{-1}, while the pre-exponential factor A was in the order of 3 times higher at 1.50×10^{12} s^{-1} or 3.37×10^{12} s^{-1}, higher than that of the reference diesel soot at 3.12×10^9 s^{-1}. The rate constant k increased with increasing temperature, and more importantly, during the dry soot oxidation, k was higher for the soot from the catalyst treated fuels.

3.3. TEM image analysis of the soot particles

Figure 5 displays typical TEM images (at 5000× magnification) of the soot particles from the present experimentation when the engine operated at speed of 3200 rpm and load of 5.5 N m. The irregularly shaped soot aggregates were composed of a number of very spherical primary particles. Comparing the three TEM images of the soot samples from the reference diesel and from the FPC treated fuels, a general trend can be seen that less particles were deposited on the TEM grids for the FPC treated fuels than for the reference diesel under the same sampling

conditions, suggesting less soot was formed when the FPC catalyst was used. This is consistent with the observation of reduced smoke emissions as discussed in Section 3.1.

The primary particle sizes (D_p) were determined by imposing circular outlines over the primary particles isolated on the TEM image. For soot particles from each type of the fuels burnt, about 1000 particles were randomly selected in total from different soot aggregates to acquire an average diameter of the primary particles ($\overline{D_p}$). This number of particles was considered to be sufficient enough to provide a statistical result because of the large data sets from different parts of the TEM grids for each particular soot sample [26,36,37]. As shown in Fig. 6, the soot primary particle sizes displayed a typical Gaussian distribution. The ($\overline{D_p}$) of the reference diesel soot was determined to be 23.9 nm, which is comparable with published data ranging from 20 to 35 nm [26,37,38]. Compared with the reference diesel soot, the soot from the two FPC treated fuels appeared to be slightly smaller with ($\overline{D_p}$) at 22.9 nm (diesel + FPC 1:10^4) and 21.2 nm (diesel + FPC 1:10^3), respectively. It is also worth noting that the primary particle size distributions were relatively narrower and more centred around the middle regions for the soot from FPC treated fuels than that for the reference diesel soot. The soot formation mechanisms in a typical compression ignition engine can be described as: condensation polymerisation of small molecules (acetylene or its higher analogues and PAH) during hydrocarbon combustion form the early stage soot precursors (nuclei); the precursors undergo several stages including surface growth, coagulation and aggregation; particle oxidation may occur at each stage in the process [1]. The eventual size of the soot primary particles depend largely on the balance between the soot formation and burnout processes [1]. The slightly smaller and narrowly-distributed primary particles for the FPC treated fuels as identified in the present study are believed to be due to the addition of FPC acts as a catalyst either interfering with the formation of the soot precursors in the early stage or accelerating the soot oxidation and burnout in the later stages.

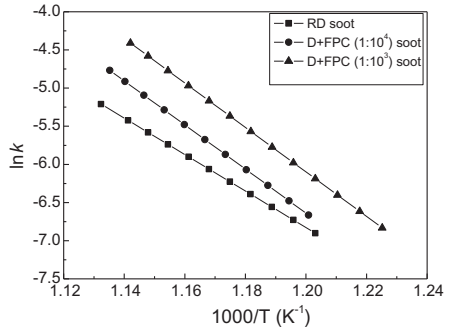

Fig. 4. Arrhenius plots for the oxidation of the soot samples from diesel with or without the FPC catalyst.

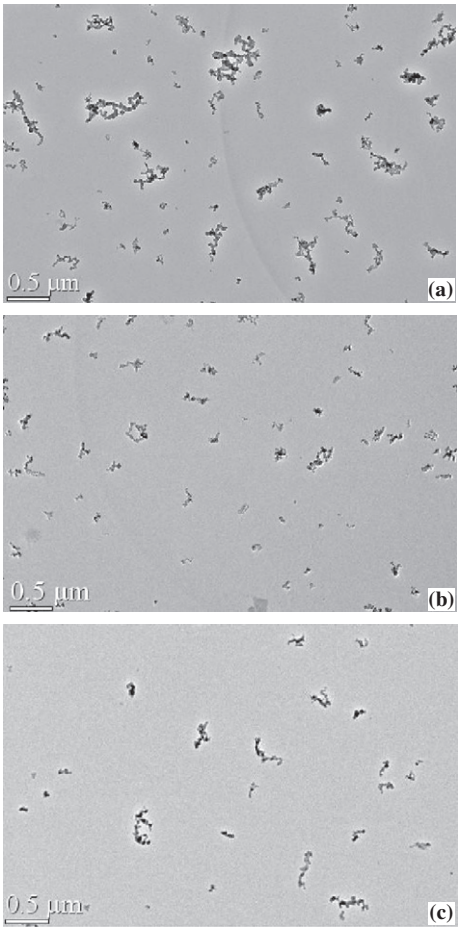

Fig. 5. Low magnification TEM images (5000×) of soot samples from (a) reference diesel, (b) diesel with FPC at 1:10^4 dosing ratio and (c) diesel with FPC 1:10^3 dosing ratio under the engine speed of 3200 rpm and 5.5 Nm load condition.

A comparison of high-resolution TEM (HRTEM) images of the soot from the reference diesel soot and the (Diesel + FPC 1:10^4) soot in Fig. 7. No significant differences in the inner structures of the two types of soot samples were observed. Both soot samples exhibited regularly spaced concentric graphitic structure with discernable nuclei regions in the core area of the structure. The lattice spacing was estimated to be of essentially the same averaged value for the two soot samples, at 0.400 and 0.402 nm, respectively. This may suggest that the interior structure of the diesel soot was not affected by the addition of the FPC catalyst in the diesel. Considering that the nuclei core arose in the early stage of the soot

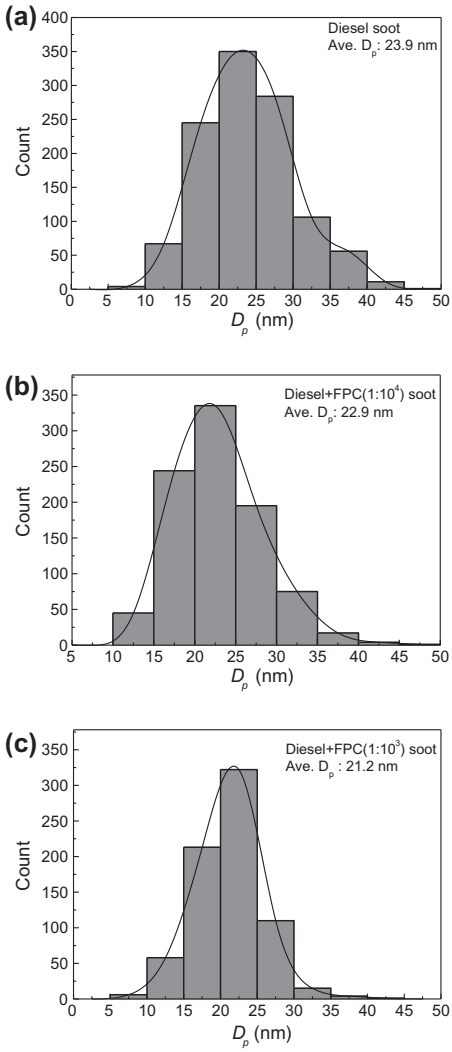

Fig. 6. The primary particle size distributions of soot samples from (a) reference diesel, (b) diesel with FPC at 1: 10^4 dosing ratio and (c) diesel with FPC 1:10^3 dosing ratio under the engine speed of 3200 rpm and 5.5 Nm load condition.

formation [1], it may be confidently concluded that rather than affecting the soot initiation process, the FPC catalyst primarily interfered the soot oxidation process which eventually led to smaller and narrowly-distributed primary particle sizes. This postulation is consistent with Hahn's work on diffusion flames [14].

4. Conclusions

A systematic study has been carried out to investigate the effect of an iron-based homogeneous combustion catalyst on the characteristics

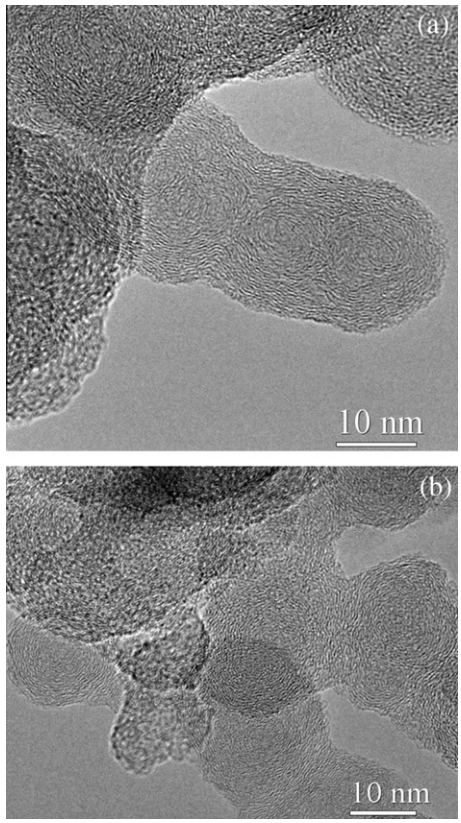

Fig. 7. High-resolution TEM images (250,000×) of soot particles from (a) reference diesel and (b) diesel with FPC at 1: 10^4 dosing ratio.

of the soot particles emitted from a diesel engine. The engine smoke tests yielded a remarkable reduction in the overall soot emissions, particularly under inefficient engine modes. Depending on the catalyst dosing ratio, the observed reductions in the soot emissions ranged from 7.3% to 39.5% under the tested conditions. The TGA tests confirmed that the soot samples from the catalyst treated fuels had higher oxidation reactivities as indicated by their lower ignition temperatures and faster oxidation rates than those from the reference diesel. The increase in soot reactivity is due to the catalytic effect of iron present in the soot from the catalyst treated diesel as this tendency was more obvious with increasing the catalyst dosage ratio. Further kinetic analysis revealed an increase in the oxidation rate constant k and pre-exponential factor A for the soot from the catalyst treated fuels. The soot particles from the catalyst treated fuels were also smaller and consisted of narrowly-distributed primary particles as identified using the TEM imaging technique. The high-resolution TEM revealed similar graphitic structures in the inner nuclei core areas of the soot particles from fuels with or without the catalyst.

This suggests that, rather than affecting the early soot formation process, the homogeneous combustion catalyst could be more involved in the soot oxidation process, which was responsible for the observed variations in the primary particle sizes and distributions of the soot.

Acknowledgements

This research has been supported by the Australian Research Council under the ARC Linkage Projects Funding Scheme (Project ID: LP0989368) in partnership with Fuel Technology Pty. Ltd. and BHPBilliton Iron Ore Pty. Ltd. The authors would also like to acknowledge the technical support from the Centre for Microscopy, Characterisation and Analysis at The University of Western Australia.

References

[1] J.B. Heywood, *Internal Combustion Engine Fundamentals*, McGraw-Hill, New York, 1988, pp. 42–648.
[2] D.B. Kittelson, *J. Aerosol Sci.* 29 (5–6) (1998) 575–588.
[3] A.C. Lloyd, T.A. Cackette, *J. Air Waste Manage.* 51 (6) (2001) 809–847.
[4] B. Hemmerich, *J. Aerosol. Sci.* 36 (7) (2005) 896–932.
[5] M. Riedl, D. Diaz-Sanchez, *J. Allergy Clin. Immunol.* 115 (2) (2005) 221–228.
[6] W. Knecht, *Energy* 33 (2) (2008) 264–271.
[7] J.B. De Andrade, N.M. Ribeiro, A.C. Pinto, C.M. Quintella, G.O. Da Rocha, L.S.G. Teixeira, *Energy Fuel* 21 (4) (2007) 2433–2445.
[8] H. Burtscher, U. Matter, G. Skillas, *J. Aerosol. Sci.* 30 (Supplement 1) (1999) S851–S852.
[9] G. Skillas, Z. Qian, U. Baltensperger, U. Matter, H. Burtscher, *Combust. Sci. Technol.* 154 (2000) 259–273.
[10] L. Witzel, P. Moszkowicz, G. Claus, *Fuel* 74 (12) (1995) 1881–1886.
[11] J. Lyyranen, J. Jokiniemi, E. Kauppinen, *J. Aerosol. Sci.* 33 (7) (2002) 967–981.
[12] M.R. Zachariah, H.J. Jung, D.B. Kittelson, *Combust. Flame* 142 (3) (2005) 276–288.
[13] T. Hirasawa, C.J. Sung, Z.W. Yang, A. Joshi, H. Wang, *Combust. Flame* 139 (4) (2004) 288–299.
[14] D.W. Hahn, K.B. Kim, K.A. Masiello, *Combust. Flame* 154 (1–2) (2008) 164–180.
[15] N.D. Marsh, I. Preciado, E.G. Eddings, A.F. Sarofim, A.B. Palotas, J.D. Robertson, *Combust. Sci. Technol.* 179 (5) (2007) 987–1001.
[16] W.R. May, E.A. Hirs, *11th Diesel Engine Emissions Reduction Conference*, Chicago, 2005.
[17] R. Anand, G.R. Kannan, R. Karvembu, *Appl. Energy* 88 (11) (2011) 3694–3703.
[18] J.H. Song, J.G. Wang, A.L. Boehman, *Combust. Flame* 146 (1–2) (2006) 73–84.
[19] M.W. Shayeson, *SAE Paper No.* 670866, 1967.
[20] A. Braun, F.E. Huggins, K.E. Kelly, B.S. Mun, S.N. Ehrlich, G.P. Huffman, *Carbon* 44 (14) (2006) 2904–2911.
[21] D. Zhang, *7th Asia-Pacific Conference on Combustion*, Taiwan, 2009.
[22] M. Zhu, Y. Ma, D. Zhang, *Energy* 36 (10) (2011) 6004–6009.
[23] Y. Ma, M. Zhu, D. Zhang, *The Australian Combustion Symposium, Newcastle (Australia)* (2011).
[24] G.A. Stratakis, A.M. Stamatelos, *Combust. Flame* 132 (1–2) (2003) 157–169.
[25] R.A. Dobbins, C.M. Megaridis, *Langmuir* 3 (2) (1987) 254–259.
[26] J.Y. Zhu, K.O. Lee, A. Yozgatligil, M.Y. Choi, *Proc. Combust. Inst.* 30 (2005) 2781–2789.
[27] M. Lapuerta, F. Oliva, J.R. Agudelo, A.L. Boehman, *Combust. Flame* 159 (2012) 844–853.
[28] S. Mosbach, M.S. Celnik, A. Raj, et al., *Combust. Flame* 156 (6) (2009) 1156–1165.
[29] W. Hai, *Proc. Combust. Inst.* 33 (1) (2011) 41–67.
[30] S. Collura, N. Chaoui, B. Azambre, G. Finqueneisel, O. Heintz, A. Krzton, *Carbon* 43 (3) (2005) 605–613.
[31] S.Y. Yorulmaz, A.T. Atimtay, *Fuel Process. Technol.* 90 (7–8) (2009) 939–946.
[32] S.H. Kim, R.A. Fletcher, M.R. Zachariah, *Environ. Sci. Technol.* 39 (11) (2005) 4021–4026.
[33] F. Bonnefoy, P. Gilot, B.R. Stanmore, G. Prado, *Carbon* 32 (7) (1994) 1333–1340.
[34] N. Miyamoto, Z. Hou, H. Ogawa, *SAE Paper No.* 881224, 1988.
[35] D. Dollimore, T.A. Evans, Y.F. Lee, F.W. Wilburn, *Thermochim. Acta* 198 (2) (1992) 249–257.
[36] K. Tian, K.A. Thomson, F. Liu, D.R. Snelling, G.J. Smallwood, D. Wang, *Combust. Flame* 144 (4) (2006) 782–791.
[37] M.F. Chandler, Y. Teng, U.O. Koylu, *Proc. Combust. Inst.* 31 (2007) 2971–2979.
[38] K.O. Lee, R. Cole, R. Sekar, et al., *Proc. Combust. Inst.* 29 (2002) 647–653.